Available online at www.sciencedirect.com
SCIENCE DIRECT
ELSEVIER
Icarus 177 (2005) 89–105
ICARUS
www.elsevier.com/locate/icarus

Maps of Titan's surface from 1 to 2.5 μm

Athena Coustenis [a,*], Mathieu Hirtzig [a], Eric Gendron [a], Pierre Drossart [a], Olivier Lai [a,b], Michel Combes [a], Alberto Negrão [a]

[a] *Laboratoire d'Etudes Spatiales et d'Instrumentation en Astrophysique (LESIA), Observatoire de Paris, Section de Meudon, 5, place Jules Janssen, 92195 Meudon Cedex, France*

[b] *CFHT Corporation, 65-1238 Mamalahoa Hwy, Kamuela, Hawaii 96743, USA*

Received 16 September 2004; revised 10 December 2004

Available online 23 May 2005

Abstract

We have acquired resolved images of Titan with the adaptive optics systems PUEO/KIR at the CFHT (Hawaii) and NAOS/CONICA at the VLT (Chile). We report here on images and maps (when data at several orbital phases are available) of Titan's surface from observations taken during the last 4 years (2001–2004) in all the methane windows between 1 and 2.5 μm (namely, at 1.08, 1.28, 1.6, and 2 μm). We present the only complete maps of Titan currently available at 1.3 μm, a spectral window where Titan appears particularly bright in spectroscopy, with a resolution of about 200 km at best on the ground. Our surface maps show the bright and dark regions sharing Titan's landscape with as much detail as possible from the ground and with high contrast in most cases. From the information gathered by comparing the maps at different wavelengths we derive constraints on the ground's composition. Our results could complete/optimize the return of the Cassini–Huygens mission.

Keywords: Titan; Satellites of Saturn; Surfaces; Satellites; Infrared observations; Image processing

1. Introduction

Spectroscopy and imaging of Titan from the ground and from Earth-orbiting observatories have proven very useful in the past two decades. Indeed, it was thanks to such measurements that we have complemented the data returned by the Voyager missions, which flew by the satellite in the early 80's. In particular, the lower atmosphere and surface of Titan were first revealed to us through HST imaging (Smith et al., 1996) and by ground-based imaging with an adaptive optics system at the 3.6-m ESO-telescope (Combes et al., 1997). Later on new HST imaging (Meier et al., 2000), Infrared Space Observatory (ISO) spectroscopy (Coustenis et al., 2003, 2005), and ground-based spectroscopic measurements (e.g., Lemmon et al., 1995; Coustenis et al., 1995; Griffith et al., 1998, 2003) added new information. More recently, larger ground-based telescopes combined with adaptive optics systems allowed us to resolve Titan's disk and to recover information at different locations (Combes et al., 1997; Coustenis et al., 2001; Brown et al., 2002; Roe et al., 2002, 2004; Hirtzig et al., 2005a), with higher precision.

With the arrival of the Cassini–Huygens mission in 2004, one might ask if such measurements can still be profitable to the community. We believe so because (a) however powerful and efficient, no mission can boast not to have use for complementing information from the ground (or from space for that matter: post-Cassini missions are already being discussed) and (b) the Huygens probe will yield the surface's composition at one single area. The latter argument pleads for the necessity of acquiring ground-based measurements simultaneously with the orbiter's observations (ISS, VIMS, Radar and so on) but also points to the usefulness of ground-based observations in general and maps of Titan in particular so that the Cassini–Huygens recordings may be extrapolated

* Corresponding author. Fax: +33 1 45077469.
E-mail address: athena.coustenis@obspm.fr (A. Coustenis).

0019-1035/$ – see front matter
doi:10.1016/j.icarus.2005.03.012

to the whole disk surface. In particular, ground-based observations can provide measurements at solar phase angles not attained by Cassini (e.g., small phase angles); complementary observations for regions that are unlit (all flybys include global images and spectra before and after the close encounters; regions that are unlit can be observed within a few days on the ground); data during times the spacecraft is observing other objects to look for time-variable phenomena (cloud formation and decay); and measurements at wavelengths that are not included in spacecraft instrumentation.

We present here Titan images taken during the past four years and the inferred maps of Titan's surface trusting that this information will be of value to the future understanding of the veiled satellite.

2. Observations

This team has observed Titan with three different adaptive optics systems and five instruments from 1994 to 2004. The COME ON+ and ADONIS systems at the ESO/3.6-m telescope in Chile were used from 1994 to 2000 and the first results were published in Combes et al. (1997). Another such AO system is PUEO at the CFHT (Hawaii), which we used from 1997 until this year (January 2004) in order to image Titan at different orbital phases and using various filters. The first results with PUEO were published in Coustenis et al. (2001). In 2000, the integral field spectrograph OASIS was located at the CFHT and combined with the adaptive optics PUEO provided us with GEE (for Greatest Eastern Elongation, meaning looking at Titan's leading side) spectro-imaging data of Titan in November 2000 (Hirtzig et al., 2005a). The last instrument used by our team is the NAOS/CONICA AO system at the ESO Very Large Telescope (Yepun, Unit 1, 8 m) in Chile, which we applied to Titan in 2002 and again this year (April 2004). A first analysis of the 2002 data and the description of this instrument were included in Gendron et al. (2004).

Here we focus on the PUEO and NACO data obtained mainly in the last four years (Table 1) and containing surface contribution. A forthcoming paper (Hirtzig et al., 2005b) deals with the images showing mainly Titan's atmosphere.

2.1. PUEO/KIR and NAOS/CONICA

PUEO combined with the KIR camera has a bandpass from 0.7 to 2.5 μm and a pixel size of 0.0348″. NACO (for NAOS combined with CONICA) operates in a 0.9–5-μm bandpass with a nominal resolution of 0.01325″ per pixel. The telescope/instrument characteristics yield diffraction limits of 0.09, 0.11, and 0.15 arcsec for PUEO at 1.28, 1.64, and 2.00 μm, respectively. For NACO and for the same wavelengths, the values are: 0.039, 0.050, and 0.065″, respectively, allowing NACO Titan measurements to afford two times higher spatial resolution (as expected from the larger telescope diameter). The best resolution thus achieved on the ground features is of about 200 km for NACO at 1.3 μm and 450 km for PUEO at the same wavelength. The resolving power of the two instruments allows us to distinguish 10 and 20 independent elements (at best) in the diameter of Titan's disk for PUEO and NACO, respectively.

For more details on the instrumental configurations and the associated filters see the CFHT and VLT/Paranal Web sites.

2.2. Observational conditions

The data we analyze here refer to observations with geometries as listed in Table 2. The NACO dates correspond to Titan angular radii of 0.44″ for 2002 and 0.37″ for 2004. The PUEO data correspond to apparent radii of 0.37, 0.43, and 0.44″ for 2001, 2002, and 2004, respectively. This explains the variations in Titan's size apparent on the figures herein (as on Fig. 1 for instance) even if Titan is observed with the same instrument.

As listed in the logbook (Table 1) NACO images suffered occasionally from poor seeing conditions. Indeed the seeing was around 2 arcsec in 2002, with the optimal conditions (around or better than 1″ for all wavelengths) on the last night. In 2004, the seeing was better, but the wind was too strong to allow us to acquire many images. Nevertheless, the few we managed to harvest afford a good seeing of around 0.6 arcsec. In comparison, PUEO images did benefit from a good and stable seeing (0.4″ at best).

Some of the raw images that we have obtained illustrating the different observing conditions can be seen in Fig. 1. These images have been treated for cosmetic effects (such as bad pixels, correlated noise and flatfield).

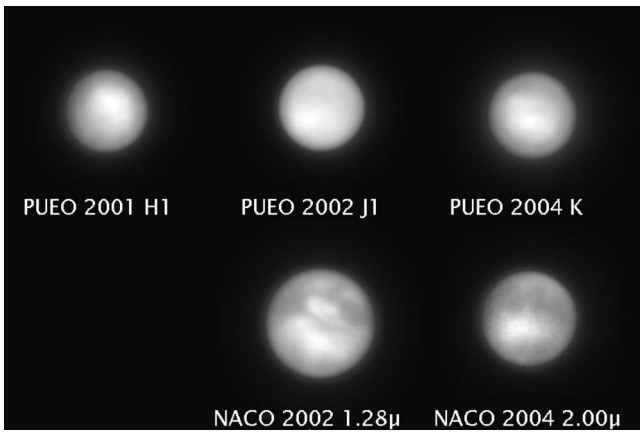

Fig. 1. An assortment of raw images of Titan taken with PUEO and NACO at the wavelengths indicated and containing surface contribution. The upper level shows our chronologically-listed PUEO images with, from left to right: H1 filter (4 December 2001, LCM = 115°), J1 filter (14 November 2002, LCM = 305°), K filter (7 January 2004, LCM = 32°). The associated wavelength and dates for NAOS/CONICA images on the lower level are respectively (26 November 2002, LCM = 212°) and (25 April 2004, LCM = 345°).

Table 1
Titan observations 2001–2004

Date	Pose time (s)	TU	Filters	Seeing	Solar phase angle
		PUEO			
07/03/2001	10.0	05h41	J2	0.8	+5.839
	90.0	06h05	J1	0.8	+5.838
	8.0	06h15	Jcont	0.8	+5.838
	40.0	07h21	H1	0.53	+5.836
	90.0	07h41	Hcont	0.7	+5.836
	180.0	08h02	Kcont	1.18	+5.835
08/03/2001	60.0	06h06	I	1.06	+5.804
	100.0	06h23	PaGamma	1.14	+5.804
	100.0	06h36	HeI	1	+5.803
	100.0	06h53	I	1	+5.803
	40.0	07h11	H1	1.07	+5.803
	100.0	07h30	Hcont	1.08	+5.802
	180.0	07h52	FeII	1.34	+5.802
04/12/2001	10.0	06h20	H1	0.65	+0.281
	90.0	06h26	FeII	0.75	+0.281
	90.0	07h07	Jcont	0.75	+0.283
	10.0	07h24	J1	0.5	+0.285
	10.0	07h30	J2	0.55	+0.285
	60.0	08h36	He1	0.63	+0.289
	60.0	08h49	PaGamma	0.49	+0.289
	10.0	09h02	H1	0.48	+0.290
	120.0	09h08	FeII	0.42	+0.291
	20.0	10h19	K	0.900	+0.295
	20.0	10h34	K′	0.8	+0.296
	240.0	10h44	H2(1-0)	0.9	+0.296
	240.0	12h26	H2(1-0)	1	+0.303
	20.0	13h01	K′	1	+0.305
	30.0	13h09	K	1	+0.305
13/11/2002	60.0	12h34	BrGamma	0.66″	−3.787
	60.0	13h20	H2(1-0)	0.66″	−3.784
	90.0	13h38	FeII	0.65″	−3.783
	30.0	14h23	H2-1	0.78″	−3.780
	30.0	14h35	H2-1	0.76″	−3.780
	20.0	15h04	J2-1	0.75″	−3.778
	20.0	15h16	J1-1	1.03″	−3.777
	30.0	15h29	H1-1	0.77″	−3.776
	90.0	15h41	FeII	0.80″	−3.775
	60.0	15h58	H2(1-0)	0.77″	−3.774
14/11/2002	20.0	11h46	J1-1	0.55″	−3.696
	20.0	12h18	J2-1	0.40″	−3.694
	30.0	12h31	H1-1	0.36″	−3.693
	30.0	12h46	H2-1	0.34″	−3.692
	90.0	13h02	FeII	0.48″	−3.691
	60.0	13h24	H2(1-0)	0.47″	−3.690
	60.0	13h38	BrGamma	0.56″	−3.689
	20.0	14h39	J1-1	0.77″	−3.685
	20.0	14h46	J2-1	0.68″	−3.684
	30.0	14h53	H1-1	0.85″	−3.684
	30.0	15h04	H2-1	0.78″	−3.683
	90.0	15h13	FeII	0.83″	−3.683
	60.0	15h24	H2(1-0)	0.87″	−3.682
	60.0	15h31	BrGamma	0.89″	−3.681
20/11/2002	20.0	12h02	J1-1	0.97″	−3.112
	20.0	12h12	J2-1	0.89″	−3.112
	30.0	12h22	H1-1	0.66″	−3.111
	30.0	12h34	H2-1	0.71″	−3.110
	90.0	12h48	FeII	0.67″	−3.109
	60.0	13h14	H2(1-0)	0.75″	−3.107

(*continued on next page*)

Table 1 (*continued*)

Date	Pose time (s)	TU	Filters	Seeing	Solar phase angle
	60.0	13h33	BrGamma	0.82″	−3.106
	20.0	14h35	J1-1	1.02″	−3.101
	20.0	14h42	J2-1	0.87″	−3.101
	30.0	14h50	H1-1	0.94″	−3.100
	30.0	15h01	H2-1	1.04″	−3.100
	90.0	15h11	FeII	1.06″	−3.099
	60.0	15h37	H2(1-0)	0.96″	−3.097
	60.0	15h56	BrGamma	0.89″	−3.096
21/11/2002	20.0	11h24	J1-1	0.71″	−3.012
	20.0	11h32	J2-1	0.68″	−3.012
	30.0	11h41	H1-1	0.84″	−3.011
	30.0	11h48	H2-1	0.75″	−3.011
	90.0	11h56	FeII	0.76″	−3.010
	60.0	12h08	H2(1-0)	0.84″	−3.009
	60.0	12h20	BrGamma	0.44″	−3.008
	20.0	13h15	J1-1	0.76″	−3.004
	20.0	13h20	J2-1	0.59″	−3.004
	30.0	13h26	H1-1	0.57″	−3.004
	30.0	13h33	H2-1	0.66″	−3.003
	90.0	13h41	FeII	0.64″	−3.003
	120.0	14h03	H2(1-0)	0.76″	−3.001
	120.0	14h27	BrGamma	0.72″	−2.999
07/01/2004	120.0	12h56	FeII	0.68″	+0.797
	60.0	13h20	H2(1-0)	0.72″	+0.799
	60.0	13h36	H2	0.80″	+0.800
	60.0	13h54	H1	1.13″	+0.801
	200.0	14h05	PaBeta	0.75″	+0.802
	200.0	14h34	H2(1-0)	0.74″	+0.805
	50.0	14h59	J2	0.73″	+0.807
08/01/2004	150.0	10h40	H2(1-0)	1.01″	+0.902
	150.0	10h59	BrGamma	0.5″?	+0.904
	6.0	11h19	K	0.6″?	+0.906
	6.0	11h23	K′	0.5″?	+0.906
	150.0	11h29	H2(1-0)	0.4″?	+0.906
	50.0	11h47	J1	0.5″?	+0.908
	40.0	11h56	J2	0.6″?	+0.909
	40.0	12h06	J	0.6″?	+0.909
	150.0	12h15	PaBeta	0.5″?	+0.910
	100.0	12h34	Jcont	0.6″?	+0.912
	150.0	12h53	H2(1-0)	0.6″?	+0.913
			NACO		
20/11/2002	10.0	06h20	NB_1.08	1.871	−3.136
	10.0	06h25	NB_1.09	2.029	−3.136
	20.0	07h20	NB_1.24	1.75	−3.132
	20.0	07h30	NB_1.28	1.729	−3.131
	80.0	07h52	NB_1.64	2.329	−3.130
	80.0	07h59	NB_1.75	2.33	−3.129
	100.0	09h05	NB_2.12	2.784	−3.125
	100.0	09h23	NB_2.17	2.437	−3.123
25/11/2002	10.0	06h21	NB_1.08	1.312	−2.606
	10.0	06h39	NB_1.09	1.267	−2.605
	20.0	07h38	NB_1.24	1.377	−2.600
	20.0	07h44	NB_1.28	1.434	−2.600
	100.0	07h51	NB_2.12	1.641	−2.599
	100.0	08h08	NB_2.17	2.121	−2.598
26/11/2002	10.0	05h50	NB_1.08	1.149	−2.497
	10.0	05h54	NB_1.09	1.076	−2.497
	10.0	05h58	NB_1.04	0.966	−2.497
	20.0	06h03	NB_1.28	0.971	−2.496

(*continued on next page*)

Table 1 (*continued*)

Date	Pose time (s)	TU	Filters	Seeing	Solar phase angle
	20.0	06h90	NB_1.24	1.028	−2.496
	100.0	06h44	NB_1.75	0.896	−2.493
	100.0	07h04	NB_1.64	0.882	−2.492
	100.0	07h26	NB_2.17	0.894	−2.490
	100.0	07h48	NB_2.12	0.918	−2.488
	20.0	08h12	NB_1.28	1.082	−2.486
	20.0	08h14	NB_1.24	0.813	−2.486
25/04/2004	100.0	22h50	NB_2.12	0.57	−5.656
	60.0	23h20	IB_2.00	0.53	−5.655
	20.0	23h30	NB_1.28	0.6	−5.655
	60.0	23h55	NB_2.17	0.64	−5.654
	60.0	00h07	NB_2.12	0.68	−5.654
	60.0	00h15	IB_2.15	0.67	−5.654

Table 2
Coordinates of Titan observations 2001–2004

Date	SEP longitude	SEP latitude	NP	Angular radius
07/03/2001	85° → 87°	−23.38°	358.10	0.377157
08/03/2001	108° → 110°	−23.41°	358.09	0.376636
04/12/2001	112° → 119°	−25.59°	356.25	0.439396
13/11/2002	283° → 287°	−26.03°	354.61	0.431365
14/11/2002	305° → 309°	−26.03°	354.61	0.431739
20/11/2002	81° → 85°	−26.07°	354.64	0.434806
21/11/2002	103° → 107°	−26.09°	354.64	0.435347
25/11/2002	189° → 191°	−26.12°	354.67	0.437106
26/11/2002	211° → 214°	−26.41°	354.68	0.437407
06/01/2004	11° → 13°	−25.25°	353.83	0.440338
07/01/2004	31° → 34°	−25.27°	353.83	0.440299
25/04/2004	344° → 346°	−25.66°	353.86	0.374961

3. Filters and processing

Our images cover several locations on Titan's disk and are taken mainly with narrow-band filters, although some additional wide-band filters were also used (see Table 3) in wavelengths ranging from 0.8 to 2.5 μm. Our data thus cover methane window locations (at 1.08, 1.28, 1.6, and 2 μm) as well as near-by spectral regions sounding mainly atmospheric levels at different altitudes. Depending on which part of the image one considers (center or limb, for instance), the altitudes probed reach the surface or are limited to some atmospheric level (as indicated in Table 3). We have used the "atmospheric" images to subtract the atmospheric contribution from the "window" images, where we expect the surface contribution to be larger but nevertheless "affected" by the atmospheric interference (mainly in the limbs). Prior to this subtraction, we use PSF observations to perform deconvolution. We then apply a model to account for haze center-to-limb effects and in most cases we sum up our images in a given filter to enhance the signal-to-noise ratio. Only then do we perform subtractions to extract information on the surface.

All of these processes are described in detail hereafter.

3.1. Point spread function and deconvolution

For each Titan observation we have also acquired PSF measurements by observing several stars. For NAOS 2002: HIC28308 (HD 40329, G5 star of V magnitude 8.18 (Oja, 1987)); for NAOS 2004: CD452690; for PUEO 2002: HD40348 (9.06 V magnitude, A0 type star (Guetter et al., 2003)); and for PUEO 2004: BD+0 1694 (aka HD 292693, 9.75 V magnitude K7 type star (Arnaud et al., 1989)), 7 Cnc (aka HD 66347, 6.841 V magnitude K0 type star (Duflot et al., 1995)), HD47358 (6.098 V magnitude G9III type star (Wielen et al., 2000)). Most of these stars are photometric standards.

Some of the PSFs we have acquired are shown in Fig. 2. With similar seeing values, the PUEO PSFs illustrate that the Airy ring is more extended at longer wavelengths (since proportional to λ/D). With a better seeing (as is the case for PUEO J1 PSF), the PSF figure is smaller and the resolution improved.

All these reference stars give a good representation of the real PSF during the acquisition of the Titan images, mainly since they were acquired in Titan's close surroundings with similar seeing, airmass, wavelength and telescope configu-

Table 3
Filters used for Titan observations

Name	λ (μm)[a]	Altitude levels probed in the image			
		Center		Limb	
		Minimum (km)	Maximum (km)	Minimum (km)	Maximum (km))
NB_1.04	1.040 ± 0.007	0	13	36	47
NB_1.08	1.083 ± 0.0075	0	8	16	43
HeI	1.083 ± 0.004	0	9	21	43
NB_1.09	1.094 ± 0.0075	11	25	46	58
PaGamma	1.094 ± 0.005	17	25	50	58
J2	1.181 ± 0.064	48	160	81	205
Jcont	1.207 ± 0.007	39	53	70	88
NB_1.24	1.237 ± 0.0075	15	29	46	60
NB_1.28	1.282 ± 0.007	0	0	16	17
PaBeta	1.282 ± 0.007	0	0	16	17
J1	1.293 ± 0.070	0	62	12	104
Hcont	1.570 ± 0.010	0	0	8	9
H1	1.600 ± 0.080	0	102	8	125
NB_1.64	1.644 ± 0.009	28	303	45	322
H2	1.640 ± 0.050	4	303	21	322
FeII	1.644 ± 0.007	28	260	45	280
NB_1.75	1.748 ± 0.013	33	300	47	318
IB_2.00	2.000 ± 0.030	0	150	9	201
K′	2.120 ± 0.170	0	240	9	261
NB_2.12	2.120 ± 0.010	0	0	17	20
H2 (1-0)	2.122 ± 0.010	0	0	17	24
IB_2.15	2.150 ± 0.030	0	193	19	214
BrGamma	2.166 ± 0.010	25	292	40	311
NB_2.17	2.166 ± 0.010	25	292	40	311
K	2.200 ± 0.168	0	320	18	340
Kcont	2.260 ± 0.030	44	310	62	328

[a] The error bars in the second column are the FWHM.

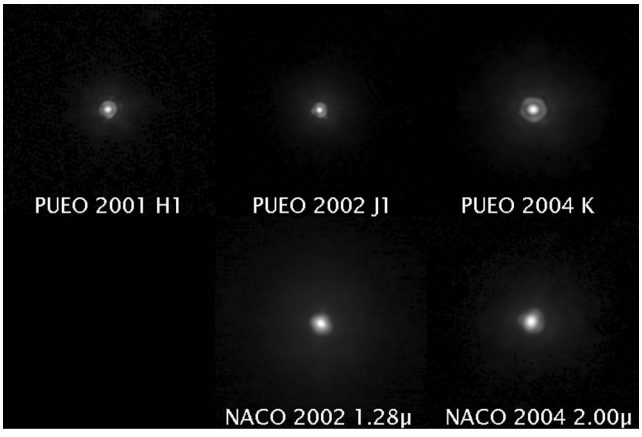

Fig. 2. The PSFs corresponding to the images of Titan shown in Fig. 1. Note the Airy rings, well visible in the upper panel PSFs and lower right.

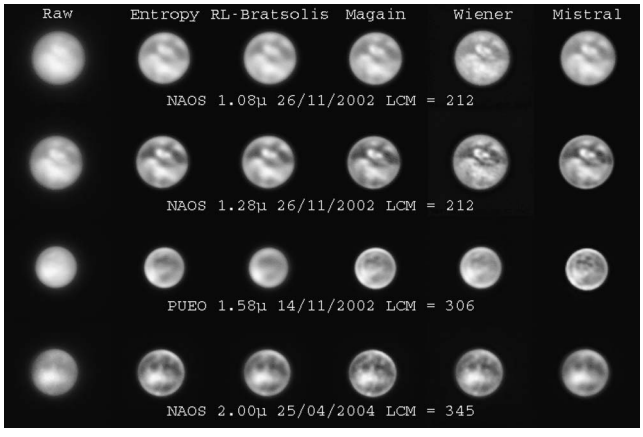

Fig. 3. Examples of different deconvolution methods applied to 4 Titan images. All methods give generally the same result when the original image is of good quality. In the following figures we adopt the Magain deconvolution method (see text).

ration. This is critical for optimizing the deconvolution. The deconvolution itself was performed with various methods: E. Bratsolis (Bratsolis and Sigelle, 2001), Magain (Magain et al., 1998), regularized or regular Lucy–Richardson for instance, and in addition tests with Wiener and entropy maximization were performed (see descriptions of the methods and intercomparisons in Combes et al. (1997), Coustenis et al. (2001), and Hirtzig et al. (2005a), and references therein).

Fig. 3 shows examples of different deconvolution methods applied to images taken at different window wavelengths.

Having tried this plethora of methods and recovered mostly the same results allows us to (a) have confidence in the features found in the resulting images and (b) need show results from only one method hereafter. Admittedly, the fact

that all methods return the same results does not necessarily mean that these results are true. Some might be deconvolution artifacts, such as a ringing effect on the disk's limb. We can ascertain that these features are not artifacts because we chose on purpose deconvolution methods based on different algorithms: for example, the Wiener method is more like a simple noise filter than an iterative reconstruction method.

Although it is true that the ringing effects are limited with this method, we opt hereafter to show our results with the Magain method. This choice is due to multiple factors. Magain returns both a good contrast (unlike the entropy one) and low noise. This may also seem to be the case with the Wiener method (Fig. 3), but the impression is due to the particularity of the stars chosen as reference for the PSF computation: the 6-magnitude stars are brighter than Titan, and as such are better resolved by the AO system. They will then be more sharply contrasted than the real PSF acquired during the Titan acquisition. This would lead to over-estimate the noise with the Wiener method (the noise is usually more smoothed out by other deconvolution methods), and all the small features present in column 5 of Fig. 3 (and not with other methods) are in fact such examples of over-estimated noise. To be more specific, the Magain method is the only one that returns diffraction-limited images regardless of the seeing. The AO system allows us to reach about 3–4 times the diffraction limit on raw images. Depending on the seeing conditions, most deconvolution methods can enhance the resolution to 1–2 times the diffraction limit, but only the Magain one will always reach the diffraction limit. This is the most important reason why we chose this latter method for our whole study.

3.2. Atmospheric haze and center-to-limb effects

Following deconvolution, we treat the surface images for center-to-limb effects. For this, we use the microphysical and radiative transfer code of Rannou et al. (2003), which is an updated version of the one described in McKay et al. (1989). This model assumes that aerosols in Titan's atmosphere are fractal-shaped (Rannou et al., 1995). The haze profile and all the parameters for this model are fully described in Rannou et al. (1995). In the calculations performed in this work we used the parameter values proposed by Negrão et al. (2004) and Coustenis et al. (2005), which is an update based on ISO near-infrared measurements (from 2.5 to 5 μm). The alterations, comparing with Rannou et al. (2003), consist in an overall increase of the haze vertical profile, calculated by the microphysical part of the model, by 40%. Also, although the altitude of the haze cut-off needed remains the same as the one used in Rannou et al. (2003), the shape of the haze vertical profile below the cut-off is slightly different. A new methane abundance near the surface of 2 instead of 8%, consistent with recent CIRS observations (Bézard et al., 2004; Flasar et al., 2005), was used in these calculations. The methane absorption coefficients used in this model are taken from a re-analysis of K. Strong and L. Giver data by R. Moreno as explained in Coustenis et al. (1995) and references therein for the 1.08- and 1.28-μm windows, and from the Hilico et al. (1994) database at and beyond 1.6 μm.

We apply this model to evaluate the effect of the haze overlying Titan's surface and correct for it. The model returns the normalized intensity from the center of the image and we apply this to our images (see Combes et al., 1997, for details). We then hopefully correct for any limb brightening or darkening in our images prior to subtraction.

Our model admittedly treats Titan's haze as homogeneously distributed over the disk, but our atmospheric images (shown on our Web site http://www.lesia.obspm.fr/planeto/Titan/Titan_sol_ao/Index.html, and see also Gendron et al., 2004) clearly show that any strong haze latitudinal variations in the later years are confined in Titan's northern or southern limbs and should not affect latitudes between 60° S and 40° N with which we are concerned here. Indeed, images taken in methane bands (as for instance at 2.12 μm) show atmospheric features located near Titan's south pole which could be clouds or other meteorological phenomena (Gendron et al., 2004). A large bright such feature is located very near the pole, showing in some cases two "companions" at mid-latitudes (around 40° S), but these features (as far as our own data are concerned) are always located on the limb (Hirtzig et al., 2005b) and we have no evidence of variable atmospheric features anywhere else on Titan's disk. So that within our model's limitations we do provide an efficient correction of the overlying haze effects such as we know them and we do not anticipate a problem with "clouds" causing errors in our atmospheric subtraction technique described in the previous section and leading to the extraction of the surface contribution for each orbital phase and wavelength.

3.3. Subtraction of the atmospheric component

In order to recover information as to the altitude probed by each filter we used, we apply the microphysical and radiative transfer code described in the previous subsection.

The estimation of the altitude probed by one given filter is based on the computation of the altitude where the effective opacity (τ_{eff}) reaches 1. In an atmosphere with multiple scattering, the regular τ does not take into account photons that would be scattered downwards, and is thus less physically meaningful. Nevertheless this singular value does not convey a satisfactory meaning because it is possible that for some wavelength within the filter bandwith we effectively reach the surface. Thus, besides the averaged value, for each filter, or altitude probed, we also present in Table 3 the lowest altitude level probed in the limit of the FWHM of the filter and which basically indicates whether the surface can be observed or not through this filter and for two cases: the center and the edge of the image.

As shown in Table 3, our narrow-band filters probe different atmospheric levels all the way down to the surface.

These filters are centered at: 1.08, 1.09, 1.28, 1.57, and 2.0 μm. From images taken in the nearby continuum (that is from spectral regions near these particular frequencies in the wings of the methane bands) we constrain the atmospheric contribution included in the "surface" filters. We then subtract the two images (according to the method described in detail in Combes et al. (1997) and also used in Coustenis et al. (2001)) to infer information on the surface contribution. The aim is to isolate this ground information as well as possible, but this is never completely achieved since the content of Titan's atmosphere is not the same in two different images. Nevertheless, this method has given good results up to now (previous such surface images of Titan have showed features confirmed by other investigations and in particular by the HST from space) and so we also use it here.

Thus, we associate our images in the following combinations:

1. HeI–PaGamma.
2. J1–J2.
3. J1–Jcont.
4. NB_1.28–NB_1.24.
5. H1–H2.
6. H1–Hcont.
7. H1–FeII.
8. K′–H2(1-0).

We can either use a narrow-band filter (cases 1, 3, 4, 6, 7, 8) or a broad-band one (cases 2 and 5) for the atmospheric contribution. The former choice allows us to eliminate a specific contribution corresponding to a definite range of altitudes, but this may not completely eliminate every atmospheric feature. On the other hand, the latter case eliminates most of the atmosphere, but large filters may contain some surface contribution even if centered in the methane band wings, thus limiting the subtraction we can apply, for fear of modifying the appearance of the surface features that are to remain. This process is even more delicate in the case of PUEO, where we deal mainly with large-band filters. This is hence a delicate operation, but in any case the resulting images are expected to contain mainly light scattered from Titan's surface, at least in the central part of the image.

4. Titan's surface in the methane windows

Because the Magain method of deconvolution effectively preserves the total flux, it is possible to apply photometry to our images and retrieve the geometric albedo of Titan at each wavelength. We have already done so in previous PUEO measurements (see geometric albedo maps in Coustenis et al., 2001) and checked the validity of our data processing in this work against ground-based spectroscopic retrievals where all observing teams agree. However, when image subtraction is applied to remove the atmospheric contribution and infer the surface albedos, discrepancies arise which have not been smoothed out until now, as will be discussed more in detail hereafter. Furthermore, different models applied to ground-based spectroscopic measurements to infer surface albedos have produced a large variety of results up to now so that we cannot validate our findings in this way. Hence, we restrain our results in presenting normalized albedo values as we did in Coustenis et al. (2001).

Besides showing independent images at various wavelengths with contribution from the surface, we have also combined our datasets where possible and extracted more or less complete Titan maps at 1.3, 1.6, and 2.0 μm from PUEO and 1.3 μm from NACO.

4.1. Images of the surface of Titan at 1.08, 1.28, and 2.0 μm with NACO

Our resulting Titan surface images with the best spatial resolution (from NACO) are shown in Figs. 4–6 with a spherical projection simulating the Titan geometry at the time of the observations. Also shown are albedo isocontours normalized at the highest intensity point.

From the images of Titan shown in Figs. 4–6 we find that Titan changes appearance with orbital phase. When we observe the leading hemisphere, we find that the images around 80–100° LCM are overall quite bright, dominated by a broad central feature (Xanadu) and surrounding darker areas (mainly to the east just above the equator (60° LCM, 5° N) and to the south-west (130° LCM, 70° S), with normalized albedos of 0.4 and 0.5, respectively). The bright equatorial feature regularly observed on all Titan GEE images is shown here at 1.08 and 1.28 μm at 79° LCM (Fig. 4) with brightest peaks located at (80° LCM, 35° S) and (90° LCM, 15° S). We find them to be 2.5 and 2 times brighter than the two darker regions respectively at 1.28 μm, while the contrast is lesser (2.0 and 1.8 for the NE and NW regions, respectively) at 1.08 μm.

As we move towards west-map (LCM higher than 200°, see Coustenis et al. (2001) for detailed references to nomenclature) on Titan, probing the trailing side, Figs. 5–6 show that the receding hemisphere of the satellite (at locations around 212° and 345° LCM) also exhibits several bright features with relatively high contrast with respect to surrounding areas. This complex topology changes our perception of Titan's trailing side as being just a uniformly "dark" place (as this has been demonstrated also in previous studies by Brown et al., 2002; Roe et al., 2002; Gendron et al., 2004). On the trailing side, as observed with NACO in 2002 at 1.08 and 1.28 μm (at 212° LCM, Fig. 5), at least 6 different brightness peaks can be distinguished: two are just above the equator (the fainter ones, on the 20th north parallel), two are just underneath it and close-by and two more can be found further to the south in a "bird-like" shape with the head to the west. The brightest features here are the furthest one to the south (220° LCM, 40° S) and the left one under the equator (220° LCM, 0° N). The darkest features on

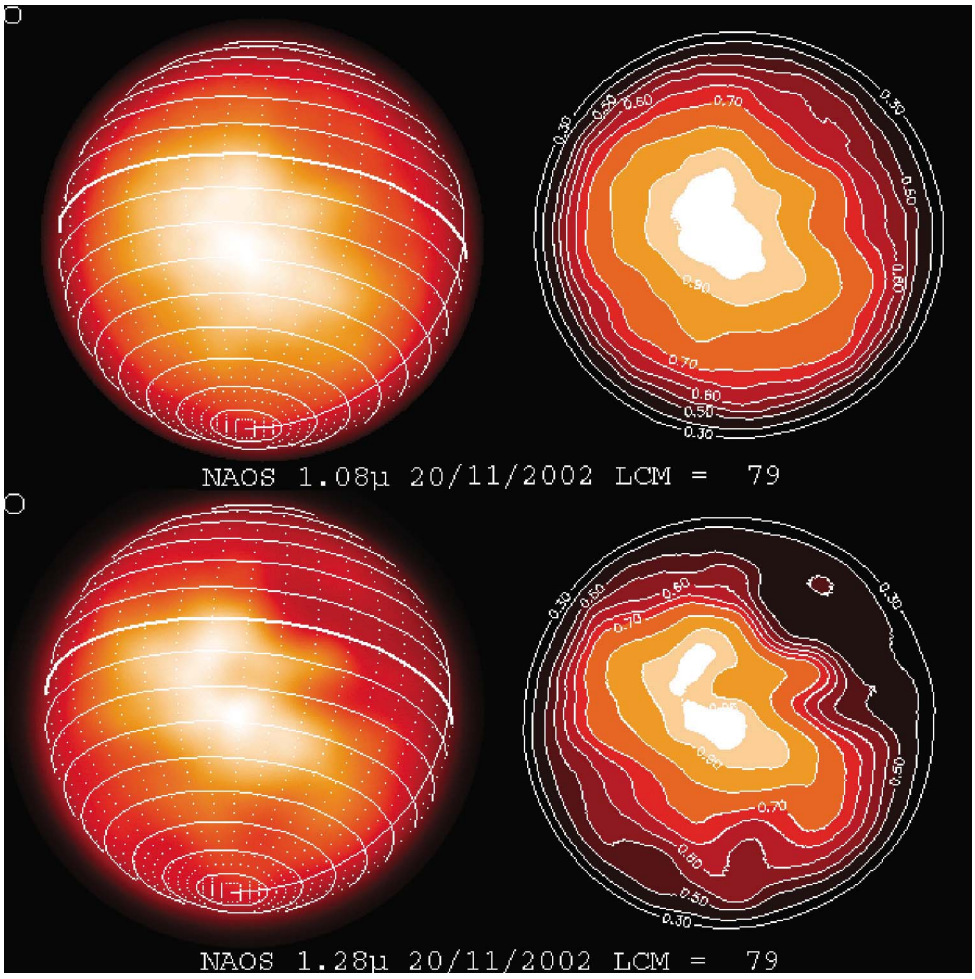

Fig. 4. Titan's surface on the leading hemisphere (LCM = 79° LCM) at 1.08 (upper part) and 1.28 µm (lower part), with the corresponding isocontour maps on the right column. The size of the resolution elements is given by the small circle in the upper left corner of each image, namely, 0.032″ and 0.038″ in diameter at 1.08 and 1.28 µm, respectively. The isocontour maps display the normalized albedo of Titan's disk, 1 for the brightest pixel. The levels drawn follow a dynamical range chosen so as to enhance the shape of the darkest and brightest features (the corresponding normalized albedo values are 0.30, 0.40, 0.5, 0.55, 0.6, 0.65, 0.7, 0.8, 0.9, and 0.95). The labels indicate the albedo value every two levels, unlabelled levels always corresponding to the average value of its two (labeled) neighbors.

the trailing side lay to the west at (260° LCM, 0° N) and to the east at (170° LCM, 10° S) with relative normalized albedos around 0.4. On this part of Titan's surface the contrast between the brightest and darkest areas as defined hereabove is of 2.5 and 1.7, respectively, at 1.28 and 1.08 µm. Again, the contrast is smaller at 1.08 than at 1.28 µm.

Our 2-µm NACO image is of excellent quality and shows in great detail Titan's surface around 345° LCM. We find here an additional significant bright feature shaped like the Australian continent located near 45° S. A serpentine of darker areas borders the equator at these longitudes. The contrast in normalized albedo between this bright region and the surrounding darker areas is quite high as shown in the isocontour plots, both at 2.0 and 1.28 µm shown in Fig. 6 for comparison. The bright area can be 2.5 and 2.0 times brighter than the dark region at (60° LCM, 0° N) and even more so when compared to the dark inlet at (50° LCM, 60° S). In this case, we have indication that the strongest contrast is to be found at 2.0 µm.

4.2. Mapping Titan's surface

Where we have several images of Titan (that is where we cover a fair number of different LCMs), we have combined our images to produce maps according to the following method.

In order to construct these maps we first compute a cylindrical projection map for each image, depending on the latitude and longitude of the sub-Earth point and the tilt of Titan's axis. All these maps are then combined together using a weighted average method: for each point, the weight corresponds to the squared cosine of the angle to the nadir. This ensures that only data near the center of Titan's disk are reliable, while data near the limbs are only used if there is no information available from another image.

Because of the processing applied to our images (and essentially the subtraction method) even the use of a photometric standard star for the PSF does not necessarily give the real photometry of Titan's disk. Thus we had to adapt

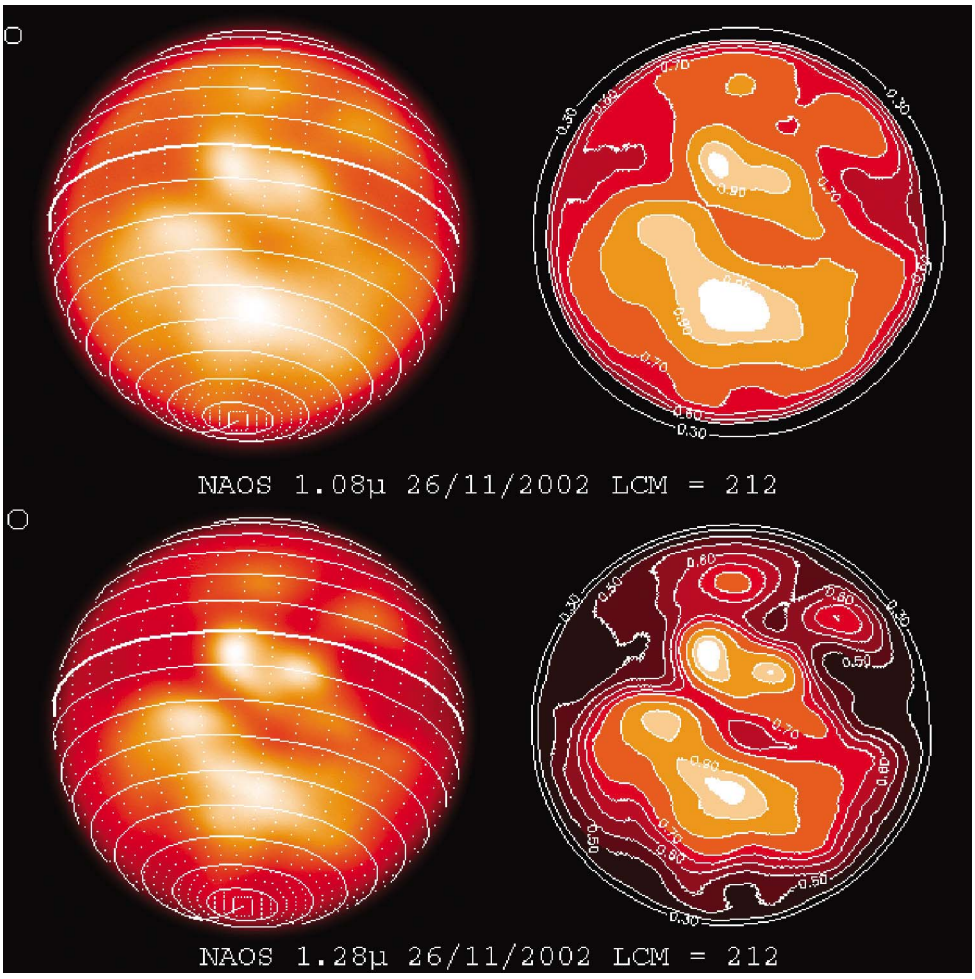

Fig. 5. Same as Fig. 4 but showing Titan's surface on the trailing hemisphere (LCM = 212°) at 1.08 µm (upper part) and 1.28 µm (lower part), along with the corresponding normalized albedo maps including Huygens' landing site. This area displays many small features, dark and bright, all over the disk, contrasting with the unique bright equatorial region on the leading hemisphere.

the photometry separately before computation of the resulting map. This is done easily for images that largely overlap with each other, where the average value of the overlapping regions is supposed to be similar. We then compute a least-square fit to recover a collection of "photometry adapting" coefficients for these overlapping data.

We retrieve the relative albedo maps shown in Figs. 7 and 8. Fig. 7 contains a map of Titan's surface at 1.28 µm with NACO (from the images shown in Figs. 4–6). Fig. 8 includes most of our PUEO data ranged in maps at three different wavelengths (1.28, 1.6, and 2 µm). The maps were put together from 2001, 2002, and 2004 data. They are consistent with and complement what we have found previously (Combes et al., 1997; Coustenis et al., 2001; Gendron et al., 2004), as well as what was reported by other teams (mainly using the HST, the Keck, etc. by (Roe et al., 2002; Brown et al., 2002); Hartung et al., 2004).

In the PUEO maps (Fig. 8) we see that the morphology of Titan's surface is quite similar but not identical at the three wavelengths. Thus, whereas the main trends are the same and we find the major bright and dark areas to be in the same locations, close investigation reveals that the bright regions near 110° LCM (Xanadu) and 345° LCM seem to extend more in latitude (in particular towards higher southern latitudes and eastern longitudes, respectively) at 1.6 µm than at 1.28 or at 2.0 µm. In the case of the latter, this could be explained by the lack of images in K′ near 10° LCM, but since we find the same behavior at 1.28 µm, we think that there may be real color differences to be found in these maps of Titan.

Another remark in this sense that one can make from the PUEO maps is that the bright spot at 45° S and near 345° LCM appears brighter at 2.0 µm than at 1.28 or 1.6 µm, similarly to what is observed in the NACO images (Fig. 6). The contrasts in other parts of the surface seem to confirm this tendency.

We have plotted in Fig. 9 an extract of the PUEO maps at 1.28, 1.6, and 2.0 µm of the region of the leading hemisphere, with an additional projection from one image taken in December 2001 at 1.08 µm (filter HeI).

The general shape of the bright area shown here changes slightly to the west and the brightest spot in Xanadu appears

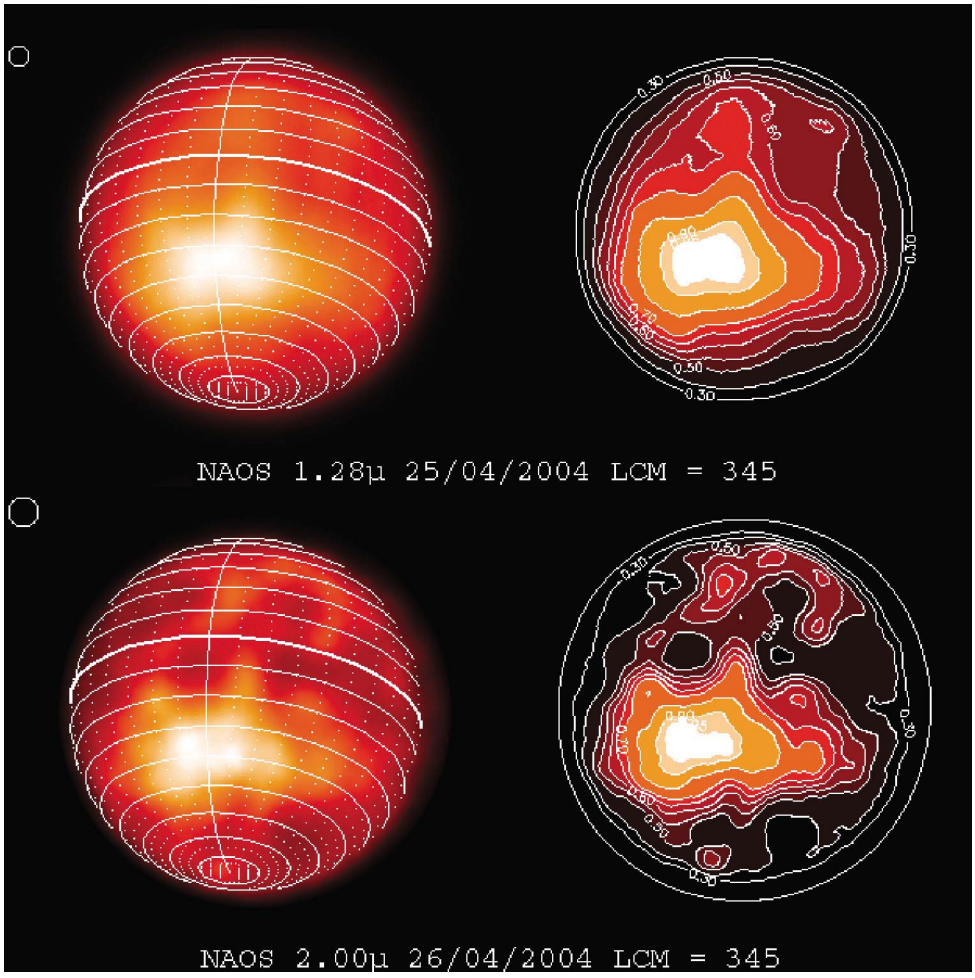

Fig. 6. Same as Fig. 4 but for Titan's surface at LCM = 345 and as seen at 1.28 and 2.0 µm. At 2.0 µm, the resolution element now spans 0.060″ in diameter, but the normalized albedo maps still show many details in the darker areas along the equator, above the "Australia-like" southern continent lying near 45° S, and which is actually an extension of the bright Xanadu region near 100° LCM.

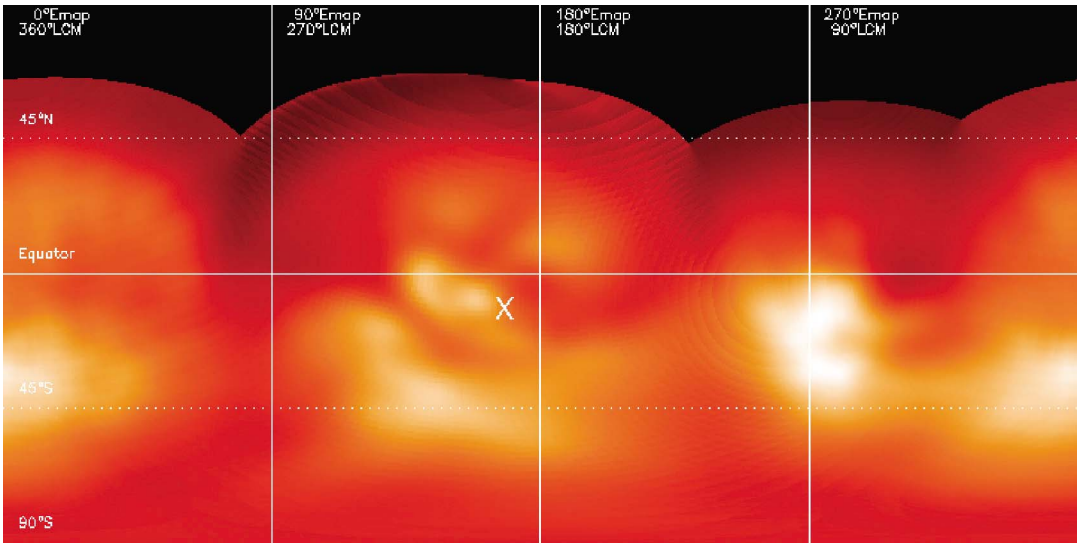

Fig. 7. Map of Titan's surface at 1.3 µm with VLT/NACO. The region between 200° and 260° LCM was very efficiently imaged by NACO on the night of November 26, 2004, when the seeing conditions were optimal. This area had rarely been observed in the past and is generally lacking in our PUEO observations. The Huygens probe has landed at (192° LCM, 10° S) indicated with an X on the map. The resolution element here is about 200 km. Our lack of optimal data near 120° LCM do not allow us to efficiently complete the map of the bright area region near 100° LCM.

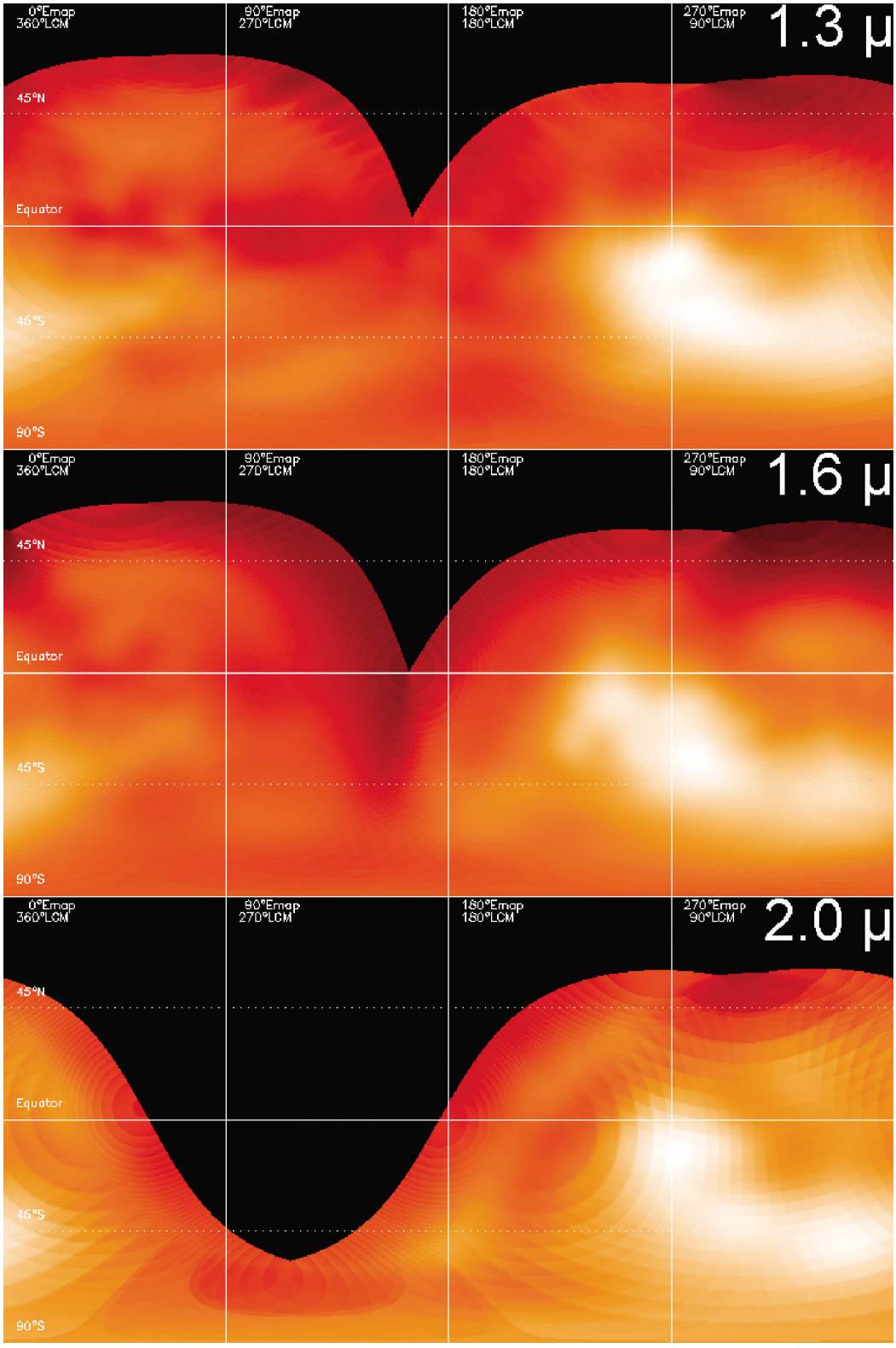

Fig. 8. Partial maps of Titan's surface acquired with PUEO from 2001 to 2004 at 1.3 (upper panel), 1.6 (middle panel) and 2.0 μm (lower panel). The maps are similar but not identical, leaving room for either processing errors or/and for real differences in the contrast observed at different wavelengths on Titan's surface, diagnostic of the spectral behavior of Titan's surface composition (see text). Besides the main bright equatorial region note the bright "offspring" emerging from its lower eastern part (60° LCM, 45° S) and extending eastward all the way to 300° LCM. The resolution elements in these maps are of about 450, 600, and 700 km, respectively, for 1.3, 1.6, and 2.0 μm.

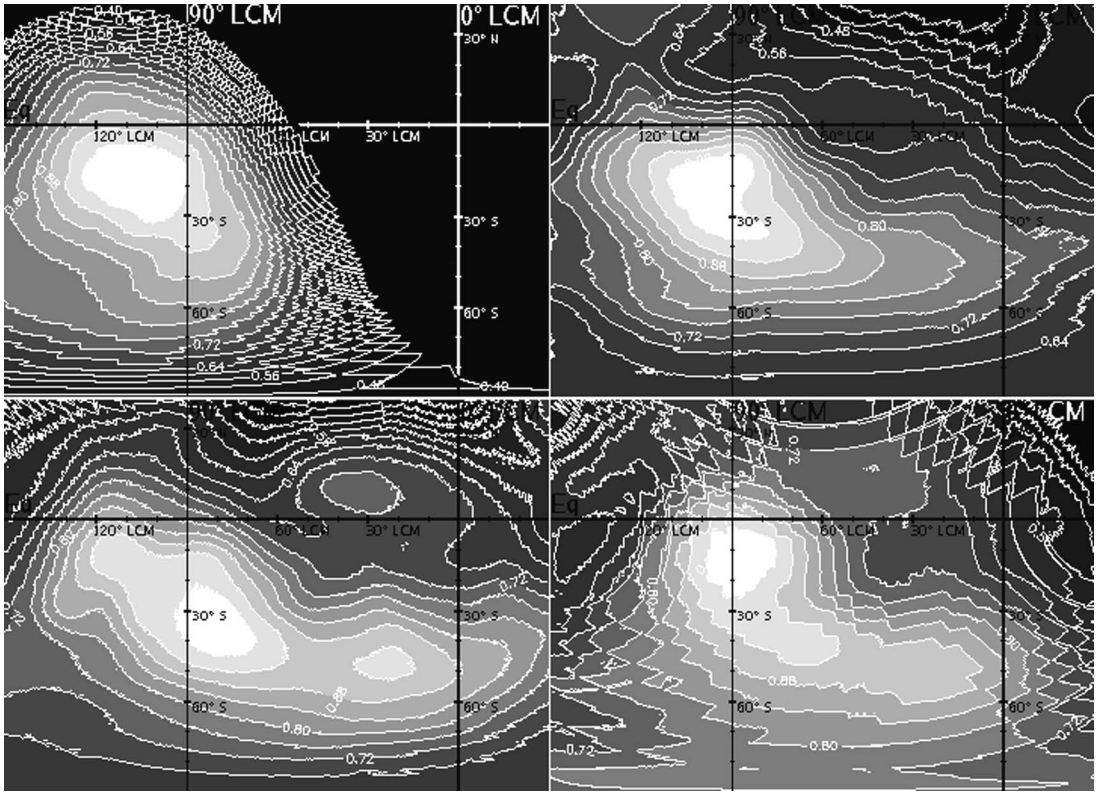

Fig. 9. Normalized albedo isocontour maps of Titan's leading side (the brightest point returns a surface albedo value of 1) at four wavelengths: 1.08 (upper left), 1.28 (upper right), 1.6 (lower left) and 2.0 μm (lower right). The brightest points at 1.3 μm are located at (90° LCM, 15° S) and (80° LCM, 35° S), whereas at 1.6 μm the brightest area can be found at (80° LCM, 35° S). The longer wavelengths show a more eastwards-extended bright region.

to be definitively one and located at (80° LCM, 35° S) at 1.6 and 2.0 μm, whereas at 1.08 and 1.28 μm there seem to be two equally bright poles (at 90° LCM, 15° S and near 80° LCM, 35° S). This second (northern) bright peak at 1.08 and 1.28 μm appears to be about 10% fainter in the 1.6-μm image. These variations confirm findings near GEE pertaining also to this region by Coustenis et al. (2001) from 1998 measurements. This change in appearance of the bright Xanadu region is significant here, since the resolution elements for PUEO maps span about 10° × 10° and 13° × 13° (450 × 450 km at 1.28 and 600 × 600 km at 1.6 μm), while the position of the bright features on Xanadu changes by some 20°. The same is true for the extension to eastern longitudes of Xanadu, that is the other bright area near 45° S and seen centered at 345° LCM, which also appears more pronounced on our PUEO maps at 1.6 and 2.0 μm than at 1.28 μm (the spatial resolution at 2.0 μm is about 700 km). Our restriction to one image projected at 1.08 μm does not allow us to infer the contrast at this wavelength.

The albedo isocontours found in Fig. 9 indicate that the contrast between the dark and the bright areas is lower at 1.08 than at 1.28 μm (again in agreement with what we find from NACO images). From this figure and from Fig. 8 of Coustenis et al. (2001), it also appears that the contrasts at 1.6 and 1.28 μm are quite similar.

4.3. Considerations on the uncertainties on the albedo contrasts

The color and shape differences for the same region between the various wavelengths could be due (a) to processing errors, (b) to the important variation of the haze influence depending with the wavelength on Titan, with the effect being less pronounced at longer wavelengths, or (c) to real differences in surface composition. Hereafter we discuss the importance of factors *a* and *b* in the different cases.

The uncertainties on the isocontours shown in Figs. 4–6 are due to (a) uncertainties on the efficiency of the subtraction method, (b) correction of the center-to-limb effect and (c) intrinsic albedo variations. In the case of NACO images, we acquired images exclusively through narrow-band filters, so that we can probe down to determined altitudes, and thus remove very specific features on the images: with such a method, we cannot over-correct the surface intensity, yet we might not correct all atmospheric features. The latter case being difficult to measure, we can only compute the case for under-correction of the features definitely recognized to pertain to the atmosphere and we find it to be about 1% with NACO, representative of the sensitivity of the central features to limb correction variations. The second cause for uncertainties, namely the center-to-limb correction, pertains to the results returned by our model, whose effects we can-

not objectively measure; yet the application of the returned extinction curve on our images creates little problem, adding a 2% error bar on the measurements, which is moreover very limited by the selection of the portion of Titan's disk we study: indeed, within 60° from the nadir point, the center-to-limb effects are minimal. Finally, the larger error bars come from the variation of the normalized albedo at one given set of coordinates within the size of the resolution element. Here the normalized albedo value for the dark regions can vary by ±0.025 (the brightest area always having by definition a normalized albedo of 1). All in all, the contrasts we measure on NACO maps can vary by about ±10%.

The case is trickier with PUEO, because the maps on Figs. 8–9 suffer from the same drawbacks as the NACO ones, and in addition errors due to the fusion of the partial maps together (as described hereabove, at the beginning of Section 4.2). With a lower spatial resolution than NACO, PUEO images suffer from worse error bars when subtracting atmospheric features from narrow-band filters: they reach about 5% here. It is even worse if we use a broad-band atmospheric filter, with up to 15% error bars, with a possibility of over-correction (even if we tried to limit this). This dramatic case only occurs for the 1.28-μm map, because we could use narrow-band filters in the three other maps computation. As for NACO, also for PUEO, within the inherent model's uncertainties, the center-to-limb effect is well corrected, and the corresponding error bar does not exceed 2% for areas near the center of Titan's disk. The size of the resolution element on PUEO maps lead to ±0.08 variations on the normalized albedo of the dark regions, for the same reasons explained hereabove. The last point is very difficult to quantify: in the case of NACO isocontour images, the definition of the normalized albedo ensures that the sky background returns a null albedo, and the brightest pixel on Titan's disk pertains to an albedo of 1. In the case of PUEO projected cylindrical maps, there is no more sky background, and the intensity itself is not guaranteed by the weighted average because of the low number of overlapping regions that can constrain the intensity fit for all Titan's globe. Yet we could constrain this to a mean error bar width of 10% on Titan's leading side. This does not affect the 1.08 μm map, since there is only one image to build up the cylindrical map. In the end, the contrasts derived from the PUEO maps can vary by about ±20% at 1.08 μm, ±40% at 1.28 μm and ±30% at 1.6 and 2.0 μm.

It then seems that from our NACO and PUEO images we can infer with some certainty trends in the albedo contrasts, which we express hereafter as a ratio of the bright (B) vs the dark (D) regions as a function of wavelength. The findings from PUEO maps (with large error bars) are compatible with those from NACO images:

- $1.08 < 1.28$ μm: depending on the region studied on Titan's disk, NACO images return B/D values of 1.7 ± 0.1 at 1.08 μm and 2.5 ± 0.1 at 1.28 μm.
- $1.28 \equiv 1.6$ μm: as found in our PUEO images and also in Coustenis et al. (2001).
- $1.28 < 2.0$ μm: on the 2004 NACO images, the contrast is higher at 2.0 μm (2.5 ± 0.1) than at 1.28 μm (2.0 ± 0.1).

This means that when we compare the bright and the dark areas on Titan, their composition has to be expressed with a spectral dependence where the difference in albedo is smaller at 1.08 than at 1.28 or 1.6 μm and smaller still than that at 2.0 μm.

Hereafter we discuss the implications of our findings in the context of Titan's surface composition.

5. Discussion

Our PUEO and NACO maps are complementary in a way because the PUEO maps afford a better coverage of the leading side whereas the NACO images produce a good coverage of the trailing hemisphere. Among them, they give a fair amount of information on what Titan's surface should be like, or at least point to some combinations that are not possible.

For the purposes of the discussion in this paper, we assume as plausible candidates for Titan's surface simple components which have been invoked in Titan studies and can be reasonably expected to exist on the satellite's surface. Such constituents were discussed in Hirtzig et al. (2005a) and include: water ice, hydrocarbon ice (methane or ethane for instance), organics/tholin material, hydrocarbon liquid and eventually rocks (mainly silicates like pyroxene or olivine).

Water ice has been suggested as a major constituent on Titan's surface in many spectroscopic studies (Coustenis et al., 1995; Griffith et al., 2003), probably not pure, but mixed with other constituents, preferably dark like impurities or organics. The spectrum of water ice is bright from 1 to 1.4 μm and then shows two albedo decreases at 1.6 and 2.0 μm where this solid has strong absorption bands. Methane ice is bright at all the wavelengths with which we are concerned here (the methane ice absorption bands fall outside the methane window wavelengths, Schmitt et al., 1998). Tholins have a flat, bright spectrum in the near-IR but show a rapid and strong decrease in albedo when moving towards the visible range (going to lower micron than 1.3). A liquid hydrocarbon spectrum is generally dark (albedo < 0.05, Grundy et al., 2002, and B. Schmitt, private communication) and flat. The silicate spectra show absorption features near 1 μm. The spectra of these constituents can be found in Fig. 15 of Hirtzig et al. (2005a).

5.1. Information on the surface composition

The bright regions present in the Titan maps appear bright at all wavelengths, at least in as far as we can monitor the same features in our maps or images. We have not observed

any obvious differences in the appearance of any of the areas we observe as a function of wavelength. The dark areas tend to remain generally dark and the bright ones remain bright. Within the capacities of our detectors and the extent of the surface area covered on Titan by our images, we find that in general the structure of the morphology is quite similar when one considers the variations in brightness and contrast which could be due to the different wavelengths (which are affected differently by the atmospheric haze), the differences/imperfections in the atmospheric subtraction, deconvolution effects and so on. At least, we have not witnessed any reversals in brightness for a region (that is we have not found indication that a bright spot has become dark with a change in wavelength). This means that we have at least 4 wavelengths (of methane windows, and possibly more than that if we include our images from OASIS at 0.94 μm (Hirtzig et al., 2005a) where the bright areas faithfully appear bright and the dark regions consistently show up dark.

If the bright regions remain bright at all wavelengths, one plausible explanation could be found in the presence of relief (mountains or plateaux) on the surface of Titan, which could increase the brightness returned in the image by virtue of the decrease in methane absorption above the mountain's top. We have performed calculations that showed that no reasonable such formation (in terms of height and extent) on Titan's surface could wholly account for the observed contrasts (as shown in the profiles of Figs. 4–6), at least as far as the brightest areas are concerned (Coustenis et al., 1997). Thus, relief alone cannot explain the brightest vs dark areas ratios. For the smaller features, with weaker contrasts (up to 40%), the presence of a mountain could be sufficient to produce the observed brightness, if this mountain was 2–3 km high. (Nothing of the sort has yet been observed by Cassini, but only a very small area has been covered by the Cassini/RADAR observations (P.I. C. Elachi) around 50° N and 82° W, a long distance from the bright equatorial or southern regions.)

For the brightest regions then we require an additional component to account for the bright vs dark color differences. If the bright areas are always more or less bright, as they appear to be, then this is indication that the surface spectrum of these regions must contain no strong absorption bands near 1.08, 1.28, 1.6, or 2.0 μm and in any case our own data strongly support a "flat" spectrum between 1.28 and 1.6 μm. By looking at the spectra of plausible surface candidates for Titan (see hereabove), we find that methane/ethane ices present this characteristic. Furthermore, as noted in Coustenis et al. (2001), a study of the thermodynamical conditions on Titan shows that ethane ice could exist on a mountain summit of a few kilometers on Titan and could be maintained there under certain non-equilibrium conditions. Hence, our best suggestion for the bright regions on Titan's surface from current knowledge would be a combination of morphology (relief) and ethane ice. This hydrocarbon ice may well be combined with another material, but it seems to us that it is required to explain the persistently bright at 0.94, 1.08, 1.28, 1.6, and 2.0 μm regions.

The general statement regarding the main trends in our images (all bright areas remain bright and dark ones stay dark) affords some exceptions, where slight color changes are observed. First, there are two areas near (240° LCM, 60° S) and (30° LCM, 25° N) showing up in the 1.6 μm PUEO map and not in the 1.3 or 2.0 μm (Fig. 8), but these two locations are within the high uncertainty border areas close to where we lack data and we do not know what level of confidence we should have there. More significant are the shape and color variations observed within the leading hemisphere and concerning the Xanadu region and its extension. Thus, it appears (as one would normally expect) that no simple and unique constituent can account for all the observations.

We furthermore have also considered what our images tell us in terms of contrasts. In other words we have quantified and investigated the behavior of the bright vs dark regions within the same area as a function of wavelength.

After considering the uncertainties described in Section 4.3, from our normalized NACO surface albedos, we find that the contrast between the darker and brighter features seems to be lowest at 1.08 and highest at 2.0 μm with respect to 1.28 μm (see results in Sections 4.1 and 4.2). This trend is confirmed in our PUEO images and maps. Hence, if we believe our data it seems that the albedo contrast behavior as function of wavelength is as follows: $1.08 < 1.28 = 1.6 < 2.0$ μm. This equation can help us attempt to constrain the possible combinations of ground material on Titan.

For the bright areas we consider always hydrocarbon ice (we refer to it as C_2H_6 ice) to account for the persistent bright appearance at all considered wavelengths. It can be pure (in which case we have flat bright spectrum at 0.94, 1.08, 1.28, 1.6, and 2.0 μm) or combined with tholins, rocks or H_2O ice (or all of that). In each of the latter combination cases, a decrease in the albedo is expected at short (<1.3 μm) or at long wavelengths (1.6 and 2.0 μm) or at all of them. But the 1.28 μm albedo should remain high.

For the dark regions, the possible candidates are water ice, hydrocarbon liquid and organic/tholin material. The spectral behavior of water ice is such that it should appear dark (or at least significantly darker) at 1.6 and 2.0 μm than at 1.08 or 1.28 μm due to the strong absorption bands it exhibits at longer wavelengths. This is not what we find in our images, although we cannot really distinguish subtle color variations. Nevertheless, it seems more plausible to assume that it is the darker regions that contain water ice, most probably in combination with another constituent such as tholin material or hydrocarbon liquid (as found by radar echoes, Campbell et al., 2003), because having the option between placing it within the bright or the dark regions, one would tend to favor the latter simply for the reason that it would be easier to explain at least the 1.6 and 2.0 μm behavior. But water ice alone can obviously not explain the dark regions. On

the other hand, tholin, hydrocarbon liquid and water ice can combine in a way that would produce a spectrum with darker areas near 0.94 and 1.6 or 2 μm than at 1.08 and 1.28 μm (see Fig. 15 in Hirtzig et al., 2005a, for the spectral representation of these constituents).

When we investigate the different combinations of material for the dark (D) and the bright (B) regions and the associated contrast and compare to our results ($1.08 < 1.28 = 1.6 \leqslant 2.0$ μm) we find:

1. B = pure C_2H_6 ice vs D = pure H_2O ice: $1.08 \leqslant 1.28 < 1.6 < 2.0$ μm. This combination seems unlikely.
2. B = C_2H_6 ice + tholins vs D = pure H_2O ice: $1.08 \leqslant 1.28 < 1.6 < 2.0$ μm. Note here that at 1.08 μm the darker regions might have a higher albedo than the bright ones because the tholin would darken the C_2H_6 ice albedo and could bring it under the H_2O ice one. This combination would work within our error bars.
3. B = C_2H_6 ice + tholins vs D = H_2O ice + hydrocarbon liquid: $1.08 < 1.28 \leqslant 1.6 \leqslant 2.0$ μm. This surface composition would work and is our favorite.
4. B = C_2H_6 ice + tholins vs D = pure hydrocarbon liquid: $1.08 < 1.28 = 1.6 = 2.0$ μm. This is a possible combination.
5. B = C_2H_6 ice + H_2O ice vs D = tholins + hydrocarbon liquid: $1.08 > 1.28 > 1.6 > 2.0$ μm. This case can apparently be excluded.

Hence, from these considerations it would appear that the most plausible situations for Titan's surface differences (our data do not allow us to infer the global composition) within the simplistic model we have presented here would be 2, 3, and 4, in other words: hydrocarbon ice combined with tholin for the bright areas and water ice–hydrocarbon liquid mixtures (or each of these constituents alone) for the darker areas. The presence of rocks would cause for the contrast in albedo to decrease around 1 μm, which is not incompatible with our data.

5.2. Comparison with other Titan maps

To the best of our knowledge, our maps are the most complete existing today from the ground at 1.3 μm. We hereafter compare them and those at other wavelengths with other existing cartographies of Titan's surface obtained with other instruments from the ground or from space (AO/Keck, SDI/VLT, NICMOS/HST, and VIMS ans ISS on Cassini).

Our 1.6 μm map with PUEO compares well with the SDI/VLT map produced by Hartung et al. (2004), although it is hard to compare because their SDI map lacks data near GEE and thus does not include the bright equatorial region, which affords the highest contrast on Titan's surface maps. In the rest of the disk, however, the observed structure is the same between the two instruments (Lorenz and Lunine, 2005).

Existing Keck maps at 1.28 and 1.6 μm by adaptive optics observations from 1999 to 2003 (Roe et al., 2002; Brown et al., 2002; Bouchez, 2003; Roe et al., 2004) show very similar structure, in particular when we compare the trailing side of Titan with the two instruments. Although at lower contrast, the Keck data are consistent with our findings.

With respect to HST maps by Smith et al. (1996) and Meier et al. (2000), we find our results to be quite similar at 1.6 and 2.0 μm.

We have compared our images with the VIMS data taken on October 26, 2004, during the Ta flyby of Titan (www.vims.lpl.Arizona.edu, R. Brown, P.I., NASA Press Release PIA 06983, Sotin et al., 2004). This data shows Titan's surface at (15° S, 156° W) in a three-filter composite image which is in good agreement with the features observed in our maps, while adding impressive resolution over this area with respect to our ground-based measurements.

The similarity between the VLT/NACO 1.3 μm map and the ISS/Cassini map at 0.94 acquired also during T0 and Ta and showing the Huygens landing site (www.ciclops.org C. Porco, team-leader, NASA Press Releases PIA 06411 for T0 and PIA 06116 for Ta, Porco et al., 2005) is remarkable, including the bright extent near (0° LCM, 45° S).

Both the data presented here and the Cassini T0 and Ta maps are confined to latitudes lower than 45° N. However, we have presented in the past images extending to higher latitudes (Coustenis et al., 2001, for instance) and hence these can prove useful to complement current Cassini data.

The surface of Titan appears to be of quite complex structure and will require with no doubt several different components and complex ground-material combinations to be interpreted. We have come a long way from the impression prevailing just two decades ago that Titan was covered with a global hydrocarbon ocean. Undoubtedly the Cassini–Huygens mission will help us satisfy an appetite for novelty that Titan has accustomed us in for almost a full century now, ever since the first suggestions of an atmosphere by Comas Solà (1908) in the early 20th century.

Acknowledgments

Some of the data presented here are based on observations collected at the European Southern Observatory, Chile (ESO proposals 70.C-0588 and 73.C-0221 for guarantee time with NACO). A. Negrão is supported by the FCT Ph.D. scholarship SFRH/BD/8006/2002.

References

Arnaud, K.A., Gilmore, G., Collier Cameron, A., 1989. An atlas of stellar spectra between 2.00 and 2.45 μm. Mon. Not. R. Astron. Soc. 237, 495–511.

Bézard, B., Coustenis, A., Fouchet, T., Lellouch, E., Conrath, B., Achterberg, R., Jennings, D., Flasar, M., the CIRS Investigation Team, 2004.

Cassini–CIRS observations of Titan's equatorial region in the submillimeter range. 36th DPS Meeting, Louisville, KY. B.A.A.S 36, p. 1119. Abstract.

Bouchez, A.H., 2003. Seasonal trends in Titan's atmosphere: Haze, winds and clouds. Ph.D. thesis, California Institute of Technology, Pasadena, CA.

Bratsolis, M., Sigelle, M., 2001. A spatial regularization method preserving local photometry for Richardson–Lucy restoration. Astron. Astrophys. 375, 1120–1128.

Brown, M.E., Bouchez, A.H., Griffith, C.A., 2002. Direct detection of variable tropospheric clouds near Titan's south pole. Nature 420, 795–797.

Campbell, D.B., Black, G.J., Carter, L.M., Ostro, S.J., 2003. Radar evidence for liquid surfaces on Titan. Science 302, 431–434.

Comas Solà, J., 1908. Observations des satellites principaux de Jupiter et de Titan. Astron. Nachr. 179, 289.

Combes, M., Vapillon, L., Gendron, E., Coustenis, A., Lai, O., Wittemberg, R., Sirdey, R., 1997. Spatially resolved images of Titan by means of adaptive optics. Icarus 129, 482–497.

Coustenis, A., Lellouch, E., Maillard, J.P., McKay, C.P., 1995. Titan's surface: Composition and variability from the near-infrared albedo. Icarus 118, 87–104.

Coustenis, A., Lellouch, E., Combes, M., Wittemberg, R., McKay, C.P., Maillard, J.P., 1997. Titan's atmosphere and surface from infrared spectroscopy and imaging. In: Cosmovici, C.B., Bowyer, S., Werthimer, D. (Eds.), Astronomical and Biochemical Origins and the Search for Life in the Universe, Proceedings of IAU, Colloquium 161, pp. 227–234.

Coustenis, A., Gendron, E., Lai, O., Véran, J.-P., Woillez, J., Combes, M., Vapillon, L., Fusco, Th., Mugnier, L., Rannou, P., 2001. Images of Titan at 1.3 and 1.6 μm with adaptive optics at the CFHT. Icarus 154, 501–515.

Coustenis, A., Salama, A., Schulz, B., Ott, S., Lellouch, E., Encrenaz, Th., Gautier, D., Feuchtgruber, H., 2003. Titan's atmosphere from ISO mid-infrared spectroscopy. Icarus 161, 383–403.

Coustenis, A., Negrão, A., Salama, A., Schulz, B., Lellouch, E., Rannou, P., Drossart, P., Encrenaz, Th., Schmitt, B., Boudon, V., Nikitin, A., 2005. Titan's 3-micron spectral region from ISO high-resolution spectroscopy. Icarus. Submitted for publication.

Duflot, M., Figon, P., Meyssonnier, N., 1995. Radial velocities: The Wilson–Evans–Batten catalogue. Astron. Astrophys., Suppl. Ser. 114, 269–280.

Flasar, F.M., Achterberg, R.K., Conrath, B.J., Gierasch, P.J., Kunde, V.G., Nixon, C.A., Bjoraker, G.L., Jennings, D.E., Romani, P.N., Simon-Miller, A.A., Bézard, B., Coustenis, A., Irwin, P.G.J., Teanby, N.A., Brasunas, J., Pearl, J.C., Segura, M.E., Carlson, R., Matmoukine, A., Schinder, P.J., Barucci, A., Courtin, R., Fouchet, T., Gautier, D., Lellouch, E., Marten, A., Prangé, R., Vinatier, S., Strobel, D.F., Calcutt, S.B., Read, P.L., Taylor, F.W., Bowles, N., Samuelson, R.E., Orton, G.S., Spilker, L.J., Owen, T.C., Spencer, J.A., Showalter, M.R., Ferrari, C., Abbas, M.M., Raulin, F., Edgington, S., Ade, P., Wishnow, E.H., 2005. Titan's atmospheric temperatures, winds, and composition. Science. In press.

Gendron, E., Coustenis, A., Drossart, P., Combes, M., Hirtzig, M., Lacombe, F., Rouan, D., Collin, C., Pau, S., Lagrange, A.-M., Mouillet, D., Rabou, P., Fusco, Th., Zins, G., 2004. VLT/NACO adaptive optics imaging of Titan. Astron. Astrophys. 421, L21–L24.

Griffith, C.A., Owen, T., Miller, G.A., Geballe, T., 1998. Transient clouds in Titan's lower atmosphere. Nature 395, 575–578.

Griffith, C.A., Owen, T., Geballe, T.R., Rayner, J., Rannou, P., 2003. Evidence for the exposure of water ice on Titan's surface. Science 300, 628–630.

Grundy, W.M., Schmitt, B., Quirico, E., 2002. The temperature-dependent spectrum of methane ice I between 0.7 and 5 μm and opportunities for near-infrared remote thermometry. Icarus 155, 486–496.

Guetter, H.H., Vrba, F.J., Henden, A.A., Luginbuhl, C.B., 2003. JHK standard stars on the CIT photometric system. Astron. J. 125, 3344–3348.

Hartung, M., Herbst, T.M., Close, L.M., Lenzen, R., Brandner, W., Marco, O., Lidman, C., 2004. A new VLT surface map of Titan at 1.575 microns. Astron. Astrophys. 421, 17–20.

Hilico, J.-C., Champion, J.-P., Toumi, S., Tyuterev, V.G., Tashkun, S.A., 1994. New analysis of the pentad system of methane and prediction of the (pentad–pentad) spectrum. J. Mol. Spectrosc. 168, 455–476.

Hirtzig, M., Coustenis, A., Lai, O., Emsellem, E., Pecontal-Rousset, A., Rannou, P., Negrão, A., Schmitt, B., 2005a. Near-infrared study of Titan's resolved disk in spectro-imaging with CFHT/OASIS. Planet. Space Sci. 53, 535–556.

Hirtzig, M., Coustenis, A., Gendron, E., Drossart, P., Negrão, A., Combes, M., Lai, O., Rannou, P., Lebonnois, S., 2005b. Monitoring atmospheric phenomena on Titan. Astron. Astrophys. Submitted for publication.

Lemmon, M.T., Karkoschka, E., Tomasko, M., 1995. Titan's rotational light-curve. Icarus 113, 27–38.

Lorenz, R.D., Lunine, J.I., 2005. Titan's surface before Cassini. Planet. Space Sci. 53, 557–576.

Magain, P., Courbin, F., Sohy, S., 1998. Deconvolution with correct sampling. Astrophys. J. 494, 472.

McKay, C.P., Pollack, J.B., Courtin, R., 1989. The thermal structure of Titan's atmosphere. Icarus 80, 23–53.

Meier, R., Smith, B.A., Owen, T.C., Terrile, R.J., 2000. The surface of Titan from NICMOS observations with the Hubble space telescope. Icarus 145, 462–473.

Negrão, A., Coustenis, A., Lellouch, E., Rannou, P., Maillard, J.P., 2004. Ground-based observations of Titan's near-infrared windows. In: 36th DPS Meeting, Louisville, KY. B.A.A.S 36, p. 1120. Abstract.

Oja, T., 1987. UBV photometry of stars whose positions are accurately known. Astron. Astrophys. 71 (Suppl. Ser.), 561–564.

Porco, C.C., Baker, E., Barbara, J., Beurle, K., Brahic, A., Burns, J.A., Charnoz, S., Cooper, N., Dawson, D.D., Del Genio, A.D., Denk, T., Dones, L., Dyudina, U., Evans, M.W., Fussner, S., Giese, B., Grazier, K., Helfenstein, P., Ingersoll, A.P., Jacobson, R.A., Johnson, T.V., McEwen, A., Murray, C.D., Neukum, G., Owen, W.M., Perry, J., Roatsch, T., Spitale, J., Squyres, S., Thomas, P., Tiscareno, M., Turtle, E.P., Vasavada, A.R., Veverka, J., Wagner, R., West, R., 2005. Imaging of Titan from the Cassini spacecraft. Nature 434, 159–168.

Rannou, P., Cabane, M., Chassefiere, E., Botet, R., McKay, C.P., Courtin, R., 1995. Titan's geometric albedo: Role of the fractal structure of the aerosols. Icarus 118, 355–372.

Rannou, P., McKay, C.P., Lorenz, R.D., 2003. A model of Titan's haze of fractal aerosols constrained by multiple observations. Planet. Space Sci. 51, 963–976.

Roe, H.G., de Pater, I., Macintosh, B.A., McKay, C.P., 2002. Titan's clouds from Gemini and Keck adaptive optics imaging. Astrophys. J. 581, 1399–1406.

Roe, H.G., de Pater, I., Gibbard, S.G., Macintosh, B.A., Max, C.E., Young, E.F., Brown, M.E., Bouchez, A.H., 2004. A new 1.6-μm map of Titan's surface. Geoph. Res. Lett. 31, L17–L20.

Schmitt, B., Quirico, E., Trotta, F., Grundy, W.M., 1998. Optical properties of ices from UV to infrared. In: Schmitt, B., de Bergh, C., Festou, M. (Eds.), Solar System Ices. In: Astrophys. Space Sci. Library, vol. 227. Kluwer Academic, Dordrecht, pp. 199–240.

Smith, P.H., Lemmon, M.T., Lorenz, R.D., Sromovsky, L.A., Caldwell, J.J., Allison, M.D., 1996. Titan's surface revealed by HST imaging. Icarus 119, 336–349.

Sotin, C., 21 colleagues, 2004. Titan's surface seen by VIMS/Cossini. In: American Geophysical Union, Fall Meeting 2004, San Francisco, CA, USA. Abstract.

Wielen, R., Schwan, H., Dettbarn, C., Lenhardt, H., Jahreiß, H., Jährling, R., Khalisi, E., 2000. Sixth catalogue of fundamental stars (FK6). Part III. Additional stars with direct solutions. Veroeff. Astron. Rechen-Inst. Heidelberg 37, 1–308.